and 5.9972 for computational errors of 0.0944 and 0.0464%, respectively. Clearly the numerical solutions offer a high degree of accuracy.

Conclusions

A new exact solution to the Navier–Stokes equations for flow in the vicinity of the forward stagnation streamline on a sphere has been developed. These solutions describe the flowfield all of the way from the body surface to the uniform flow far from the body, in contrast to the traditional stagnation point solutions and, hence, may be used to obtain solutions for the entire range of Reynolds numbers. Solutions have been obtained for the vorticity field and the stream function field for Reynolds numbers from 10^{-2} to 10^{6}, and these solutions have been used to calculate the stagnation point pressure coefficient on a sphere for this Reynolds number range. The results provide an excellent prediction of the stagnation point pressure coefficient over the entire Reynolds number range.

References

[1]Issa, R. I., "Rise of Total Pressure in Frictional Flow," *AIAA Journal*, Vol. 33, No. 4, 1995, pp. 772–774.

[2]Van Ondhensden, B. W., "Comment on 'Rise of Total Pressure in Frictional Flow,'" *AIAA Journal*, Vol. 35, No. 2, 1996, pp. 426–427.

[3]Schlichting, H., *Boundary Layer Theory*, McGraw–Hill, New York, 1979, pp. 95–101.

[4]Homann, F., "Der Einfluss grosser Zähigkeit bei der Strömmung um den Zylinder und um die Kugel," *Zeitschrift für Angewandte Mathemik und Mechanik*, Vol. 16, No. 3, 1936, p. 153.

[5]LeClair, B. P., Hamielec, A. E., and Pruppacher, H. R., "A Numerical Study of the Drag on a Sphere at Low and Intermediate Reynolds Numbers," *Journal of the Atmospheric Sciences*, Vol. 27, No. 2, 1970, pp. 308–315.

J. C. Hermanson
Associate Editor

Symmetry Properties of the Transitional Sphere Wake

R. Mittal* and J. J. Wilson†
University of Florida, Gainesville, Florida 32611
and
F. M. Najjar‡
University of Illinois at Urbana–Champaign, Urbana, Illinois 61801

Introduction

ON the basis of previous studies,[1–11] it is reasonable to state that the various bifurcations as well as the vortex dynamics in the wake of a sphere are relatively well understood up to a Reynolds number (based on sphere diameter D and freestream velocity U_∞) of about 350. In particular, it is known that the axisymmetric, steady wake first becomes unstable to nonaxisymmetric perturbations at a Reynolds number of about 210 (Ref. 7). The next bifurcation occurs at a Reynolds number of about 277 and leads to the establishment of time-periodic shedding[10] of vortex loops. In this shedding mode vortex loops are formed precisely at the same azimuthal location in every cycle, and the wake maintains strict symmetry at every time instant about a fixed plane that passes through the wake centerline.[5] The orientation of the symmetry plane is determined in simulations by the initial conditions. Studies[5,8] also indicate that strict planar symmetry is lost somewhere between 350 and 375, but to date there is no clear consensus on the nature of the vortex formation process at these higher Reynolds numbers. Most studies[9,10] implicitly assume that the vortex loops do not have any preferred orientation and that the time-averaged wake is axisymmetric about the wake centerline.

The objective of this Note is to use direct numerical simulation (DNS) data of flow past a sphere to analyze the symmetry properties of the time-averaged wake in the range $500 \leq Re \leq 1000$. To this end, an accurate Fourier–Chebyshev spectral collocation method has been used for computing three-dimensional, unsteady, viscous incompressible flow past a sphere where time advancement is through a second-order-accurate time-split scheme. The current solver has been validated extensively[4] in the Reynolds number range $50 < Re < 500$ against established experimental data. A detailed description of the solver and validation study, as well as other computed results can be found in Refs. 4, 5, and 12.

Results of DNS at three Reynolds numbers (500, 650, and 1000) are reported here. The outer domain size for these simulations is $25D$, and the grid for each simulation is chosen so as to ensure at least five orders of magnitude decay in the wave-number spectra of the flow variables. This results in a grid with 6.4×10^5 (1.3×10^6) collocation points for the $Re = 500$ ($Re = 1000$) simulation. Initially, a mean axisymmetric flow is obtained. Subsequently, a small perturbation in the form of a random (white noise) azimuthal slip velocity is provided on the sphere surface for a short time. This perturbation is random in space and therefore does not have a preferred spatial structure or orientation. The disturbance grows in time as a result of the inherent instability of the flow and eventually saturates, at which point data are extracted for analysis.

Discussion of Results

The force on the sphere is decomposed into three components: the drag force F_d, which acts in the streamwise (x-) direction, and the two components of the side force (F_y and F_z), which act perpendicular to the drag force. The magnitude of the side force can be computed as $F_s = \sqrt{(F_y^2 + F_z^2)}$. Figure 1 shows the variation of the drag C_d and side force C_s coefficients with time. The mean values of the drag coefficient for $Re = 500$, 650, and 1000 are computed to be 0.56, 0.52, and 0.47, respectively, and these are in very good agreement with experiments.[13] The side-force coefficients show a complex behavior with magnitudes that are roughly an order smaller than those of the drag coefficient.

Based on all of the data that have been analyzed,[14] the dominant nondimensional shedding frequency (fD/U_∞, where f is the shedding frequency) lies in the range from 0.17 to 0.19 for the entire range of Reynolds numbers simulated here, and this is in line with experiments.[10] In addition, the current simulations indicate the presence of a low frequency in the near wake with nondimensional frequency equal to 0.05 for all of the three Reynolds numbers investigated. Despite similar previous observations,[8,9,11] the dynamics associated with this low frequency are not currently well understood.

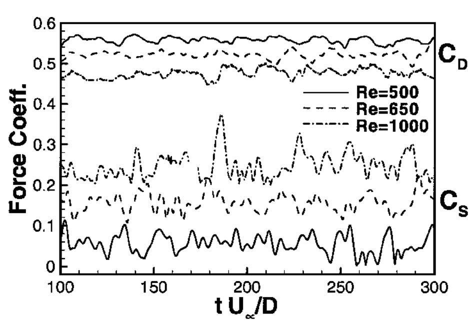

Fig. 1 Temporal variation of drag and side-force coefficients. The side-force coefficients for $Re = 650$ and 1000 have been offset in the vertical direction by +0.1 and +0.2 respectively.

Received 5 May 2001; revision received 6 November 2001; accepted for publication 12 November 2001.

*Assistant Professor, Department of Mechanical Engineering; currently Assistant Professor, Department of Mechanical and Aerospace Engineering, George Washington University, Washington, DC 20052. Member AIAA.

†Graduate Student, Department of Mechanical Engineering.

‡Principal Research Scientist, Center for Simulation of Advanced Rockets. Member AIAA.

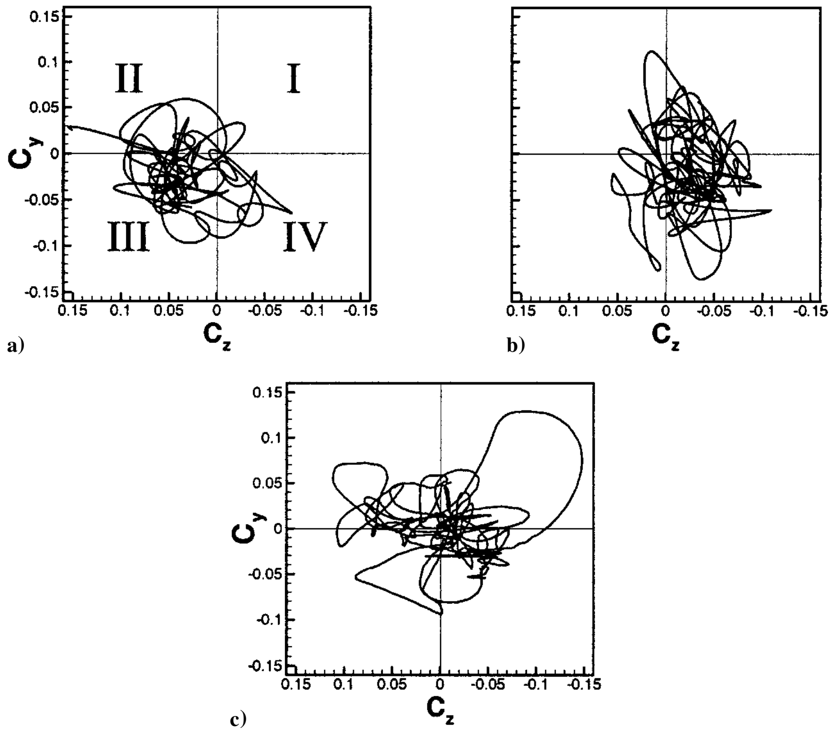

Fig. 2 Phase-plane plot of the two components of the side-force coefficient experienced by the sphere: a) *Re* = 500, b) *Re* = 650, and c) *Re* = 1000. The four quadrants have been numbered in Fig. 2a.

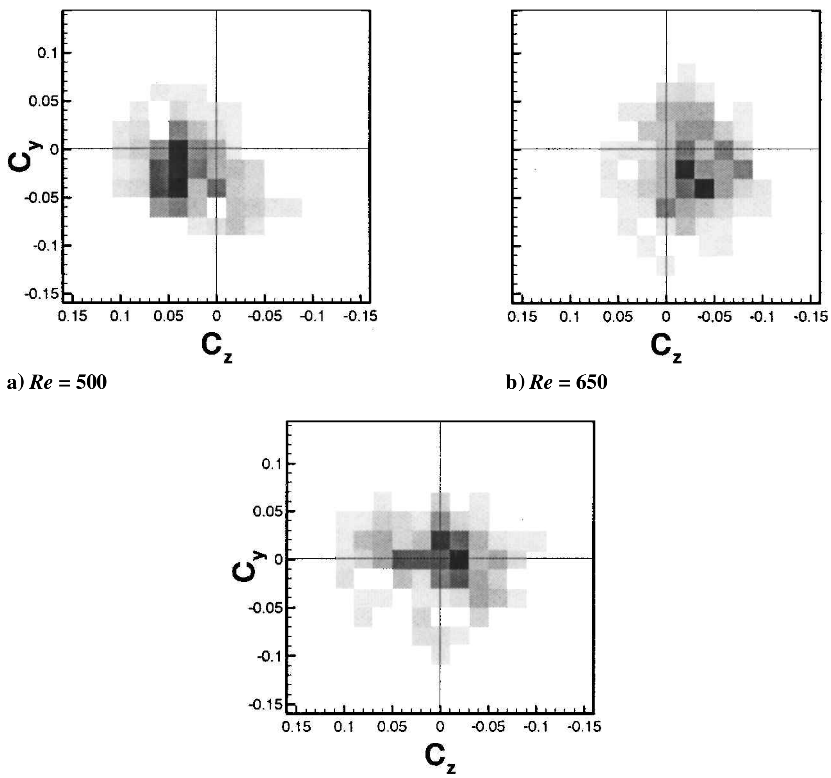

Fig. 3 Probability density function of the nondimensional side-force vector. Darker shades correspond to higher values of PDF.

In this study simulations have been integrated in time for over 300 time units (D/U_∞) and stationary-state results obtained by discarding the first hundred time units. Thus, stationary-state data and statistics presented here are over a time interval that would correspond to over 34 vortex shedding cycles and 10 cycles of the low-frequency phenomenon.

The near-wake symmetry can be explored through the phase plane plot of the two side-force coefficients C_y and C_z (Ref. 5) shown in Fig. 2. All three plots show a highly complex behavior of the

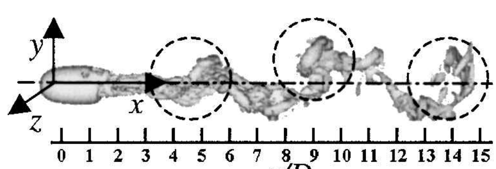

Fig. 4 Visualization of vortex structures at one time instant for *Re* = 1000. Dashed circles indicate identifiable vortex loops or rings.

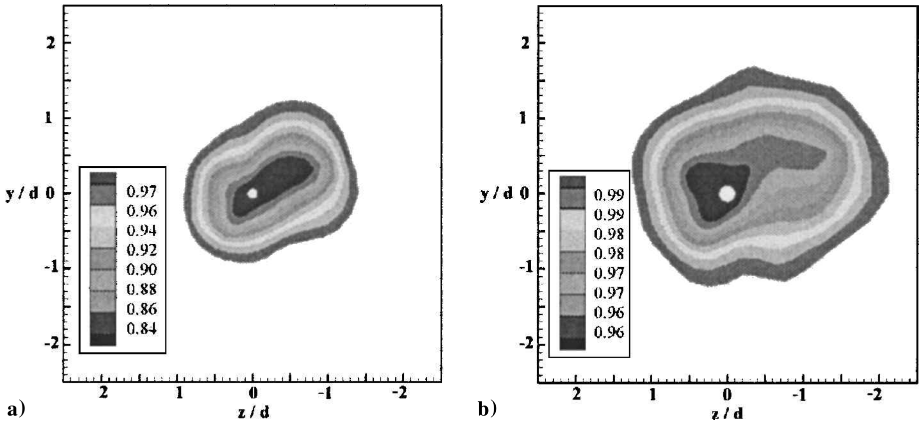

Fig. 5 Contours of time-averaged streamwise velocity in the sphere wake at selected streamwise planes in the wake for $Re = 500$: a) $x/D = 5.0$ and b) $x/D = 12.5$.

side-force vector. However, a preferred orientation of the side force in the third and fourth quadrants can easily be discerned visually for $Re = 500$ and 650 respectively, but not for $Re = 1000$. To obtain a quantitative measure of this preferential orientation, we have computed the probability density function (PDF) of the side-force vector in the phase plane. Figure 3 shows the PDF distribution, and based on this we note that the most likely values of the nondimensionalized side-force vector (C_z, C_y) are $(0.05, -0.03)$, $(-0.03, -0.03)$, and $(-0.01, -0.01)$ for $Re = 500$, 650, and 1000 respectively. This provides quantitative evidence that vortex loops formed in the near wake clearly have a preferred azimuthal orientation in this Reynolds-number range. However, with increasing Reynolds number the preference for any particular orientation diminishes, and consequently the time-averaged near wake tends to become more axisymmetric. Note that the mean side-force is nonzero, and this is in line with the behavior observed for the sphere in the strictly planar symmetric $(210 < Re < 360)$ regime.[5]

Even though vortex loops form with a preferred orientation in the near wake, it is possible that they could undergo a spiraling motion[11] as they convect downstream. In this scenario the time-averaged wake would indicate a rotation in the preferred direction with streamwise distance. Another possibility is that the vortex loops are formed with a preferred orientation in the near wake but become more randomly oriented as they convect downstream. In this case the time-averaged wake in the downstream region would tend to look axisymmetric. Figure 4 presents visualizations of the vortex structures[4,5,12,15] in the wake for $Re = 10^3$ at one time instant. The figure shows the presence of vortex loops and rings and does not indicate any obvious spiraling motion in the vortex structures. In fact, the visualization indicate that strong vortex loops and rings are preferentially formed above the wake centerline for $Re = 1000$. Corresponding plots for $Re = 500$ and 650 also show a preferred orientation in the wake. Thus, the flow visualizations are consistent with the presence of a preferred orientation in the wake.

To analyze the long-term behavior of the wake, we have plotted contours of the time-averaged streamwise component of velocity at two different streamwise locations in the wake ($x/D = 5.0$ and 12.5) in Fig. 5. These plots indicate that the wake is far from being axisymmetric in the time-averaged sense. In fact, the plots are suggestive of a planar symmetric behavior, although the planar symmetry is not precise owing perhaps to the statistical uncertainty associated with the sample size. The most probable side-force vector is along the 30-deg line from the z direction (Fig. 3a), and this is consistent with the direction of the symmetry plane evident in Fig. 5. If the low frequency of 0.05 observed in the wake were associated with a slow rotation in the azimuthal orientation of the vortex loops, then in traversing from x/D of 5.0 to 12.5 the plane of symmetry would rotate roughly by 135 deg. However, Fig. 5 shows no significant change in the apparent plane of symmetry with streamwise distance suggesting that the preferred direction associated with the formation of the vortex loops in the near wake is maintained in the downstream wake region also. The time-averaged wakes for $Re = 650$ and 1000 also show a similar behavior indicating that the wake in this entire Reynolds-number range exhibits the same qualitative features. Thus, it can be concluded that in the range of Reynolds numbers investigated the time-averaged wake maintains a fixed preferred orientation, and neither of the two scenarios discussed in the preceding paragraph are actually observed for this flow.

Conclusions

The current simulations suggest that loss of strict planar symmetry in the sphere wake at a Reynolds number of about 360 is not immediately followed by the appearance of a statistically axisymmetric wake. Instead, the wake transitions to a mode where vortex loops are formed with a preferred orientation. There are, however, significant cycle-to-cycle variations in the orientation of the vortex loops about this preferred orientation, and this leads to a wake that is most likely to be planar symmetric in the time-averaged sense. The variation in the vortex loop orientation is highly complex with no discernable pattern, and this complexity is possibly a result of the presence of two incommensurate frequencies in the wake. The variability in the orientation of the vortex loops is also found to increase with Reynolds number. Thus, as the Reynolds number increases the preference toward any particular azimuthal orientation diminishes, and the wake is expected to slowly approach a statistically axisymmetric state. The data presented here have been sampled over a time interval large enough so as to reasonably include any topological variations that might occur over a time interval spanning up to about 34 shedding cycles and 10 cycles of the low-frequency phenomenon. Despite this relatively long sampling time, the behavior observed here will have to be confirmed over a larger time span either through experiments or numerical stability analysis. Until such investigations are undertaken, the current simulations add yet another element to our understanding of the peculiar and interesting behavior exhibited by the sphere wake.

Acknowledgment

Computer time for these simulations has been provided through a supercomputing grant from the National Center for Supercomputing Applications, Urbana, Illinois.

References

[1] Constantinescu, G. S., and Squires, K. D., "LES and DNS Investigations of Turbulent Flow over a Sphere," AIAA Paper 2000-0540, 2000.

[2] Johnson, T. A., and Patel, V. C., "Flow Past a Sphere up to a Reynolds Number of 300," *Journal of Fluid Mechanics*, Vol. 378, 1999, pp. 19–70.

[3] Magarvey, R. H., and Bishop, R. L., "Transition Ranges for Three-Dimensional Wakes," *Canadian Journal of Physics*, Vol. 39, 1961, pp. 1418–1422.

[4] Mittal, R., "A Fourier-Chebyshev Spectral Collocation Method for Simulating Flow past Spheres and Spheroids," *International Journal for Numerical Methods of Fluids*, Vol. 30, 1999, pp. 921–937.

[5] Mittal, R., "Planar Symmetry in the Unsteady Wake of a Sphere," *AIAA Journal*, Vol. 37, No. 3, 1999, pp. 388–391.

[6] Nakamura, I., "Steady Wake Behind a Sphere," *Physics of Fluids*, Vol. 19, No. 1, 1976, pp. 5–8.

[7]Natarajan, R., and Acrivos, A., "The Instability of the Steady Flow past Spheres and Disks," *Journal of Fluid Mechanics*, Vol. 254, 1993, pp. 323–344.

[8]Ormieres, D., and Provansal, M., "Transition to Turbulence in the Wake of a Sphere," *Physical Review Letters*, Vol. 83, No. 1, 1999, pp. 80–83.

[9]Sakamoto, H., and Haniu, H., "A Study of Vortex Shedding from Spheres in a Uniform Flow," *Journal of Fluids Engineering*, Vol. 112, 1990, pp. 386–392.

[10]Sakamoto, H., and Haniu, H., "The Formation Mechanism and Shedding Frequency of Vortices from a Sphere in Uniform Shear Flow," *Journal of Fluid Mechanics*, Vol. 287, 1995, pp. 151–171.

[11]Tomboulides, A. G., and Orszag, S. A., "Numerical Investigation of Transitional and Weak Turbulent Flow past a Sphere," *Journal of Fluid Mechanics*, Vol. 416, 2000, pp. 45–73.

[12]Mittal, R., "Response of the Sphere Wake to Freestream Fluctuations," *Theoretical and Computational Fluid Dynamics*, Vol. 13, 2000, pp. 397–419.

[13]Roos, F. W., and Willmarth, W. W., "Some Experimental Results on Sphere and Disk Drag," *AIAA Journal*, Vol. 9, No. 2, 1971, 285–291.

[14]Wilson, J. J., "Vortex Dynamics and Vortex Shedding Lock-On in the Wake of a Sphere," M.S. Thesis, Dept. of Mechanical Engineering, Univ. of Florida, Gainesville, FL, July 2000.

[15]Chong, M. S., Perry, A. E., and Cantwell, B. J., "A General Classification of Three-Dimensional Flow Fields," *Physics of Fluids A*, Vol. 5, 1990, pp. 765–777.

S. K. Aggarwal
Associate Editor

New Self-Referencing Pressure-Sensitive-Paint Measurement

Chelakara S. Subramanian*
Florida Institute of Technology, Melbourne, Florida 32901
and
Tahani R. Amer,† Donald M. Oglesby,‡
and Cecil G. Burkett, Jr.§
NASA Langley Research Center, Hampton, Virginia 23681

I. Introduction

FOR most pressure-sensitive paints (PSP) the intensity ratio (I_0/I) and pressure ratio (P/P_0) relationship is nonlinear at low pressures (<0.2 psia when the oxygen level is low). This nonlinearity can be attributed to variations in the oxygen quenching rates. Other studies suggest that some paints also have nonlinear calibrations at high pressures because of heterogeneous (nonuniform) oxygen diffusion and quenching. In such cases errors caused by nonlinearity in calibration could be significant if the Stern–Volmer linear equation is used. Moreover, PSPs require correction for the output intensity as a result of light intensity variation, paint coating variation, model dynamics, wind off reference pressure variation, and temperature sensitivity. Here an in-situ intensity correction method is attempted to simplify the correction procedure. A nonoxygen quenched paint [which provides a constant intensity at all pressures, called nonpressure sensitive paint (NPSP)] was used for the reference intensity I_{NPSP} with respect to which all of the PSP intensities I were measured.

PSP measurements provide a means for the recovery of global surface-pressure distributions on aerodynamic test articles.[1] A typical PSP consists of a 25–40 μm-thick reflective undercoat and a 25–40-μm thick coating of a luminophore dispersed in a binder layer. The binder is usually a polymeric material. The principle of operation of pressure sensitive paints is well described in the literature.[2–5]

Under the appropriate illumination and constant quenching rates of fluorescence and internal conversion, the intensity of the luminescence emission from the paint is inversely proportional to the oxygen concentration and, hence, the air pressure on the surface. The luminescence of PSP can be expressed in terms of the well-known Stern–Volmer relation:

$$I_0/I = 1 + KP \tag{1}$$

where I_0 is the emission at zero-oxygen level and I is the emission at any pressure P. K is assumed to be a constant. It is generally not practical to measure I_0 in the wind-tunnel environment because the tunnel would have to be pumped down to a vacuum. Instead of trying to achieve zero-oxygen conditions, the intensity of emission at "wind off" I_1 is used as the reference intensity, and the pressure at wind off is considered the reference pressure P_1. In practice, this is usually the local barometric pressure. In terms of the Stern–Volmer equation, this takes the form of the ratio of the Stern–Volmer relation for two pressures:

$$I_1/I_2 = A + BP_2 \tag{2}$$

Because luminescence intensity depends on illumination intensity, values for I are determined for each point on the wind-tunnel model at each angle of attack. The values for A and B are then determined from a plot of I_1/I_2 vs pressure, using pressure taps on the model for calibration. The accuracy of this type of calibration depends on maintaining constant and reproducible illumination at every model position. Because the light intensity at the surface of the model changes with the angle of attack, the reference intensity I_1 at every model position must be measured. To ratio correctly these wind-off measurements to the wind-on measurements, spatial registration dots must be placed on the model. These enable the wind-off and wind-on images to be aligned correctly.

The objective of this study is to develop a paint and measurement system that would not require the wind-off calibration and would correct for differences in illumination intensity over the model surface. Others have used dual luminophore PSPs to correct for light intensity variations and also temperature variations.[5–8] However, mixing different luminophores in the same paint matrix nearly always produces spectral interference between the different luminophores. If the registration dots could be prepared from paint containing a luminophore that is not quenched by oxygen, the emission from the dots can also serve as a light intensity reference. The luminophore in the registration dots should be one that is excited by the same illumination used to excite the pressure-sensing luminophores in the PSP. Theoretically, the optimum system would have the same luminophore in the registration dots as in the paint but contained in a binder that is oxygen impermeable. This way the pixel intensity at the dot can be used as the light reference intensity. Having the same luminophore in the dot would eliminate the need for a filter wheel or filter shuttle on the camera in order to observe different wavelengths of light. However, practical binders have some oxygen permeability, and even a small amount of quenching of the luminophore in the dot would cause serious errors. It is easier to find a luminophore, which is not quenched by oxygen, than it is to find a totally impermeable polymer paint matrix. This would mean that the target dots would emit at a different wavelength of light than the PSP. Therefore, the reference luminophore should emit at a wavelength sufficiently different from that emitted by the pressure sensing luminophore to be resolved with different filters over the camera lens. Instead of taking the ratio of wind-off intensity to the wind-on intensity, the ratio of the intensity of emission from the nearest registration mark to

Presented as Paper 2000-2526 at the AIAA 21st Aerodynamic Measurement Technology and Ground Testing Conference, Denver, CO, 19–22 June 2000; received 14 April 2001; revision received 16 October 2001; accepted for publication 3 November 2001.

*Professor of Aerospace Engineering, 150 W. University Boulevard; subraman@zach.fit.edu. Associate Fellow AIAA.

†Aerospace Engineer, Instrument Status Data Block.

‡Analytical Chemist, Instrument Status Data Block.

§Technologist, Instrument Status Data Block.